

**Insights into pressure tunable reaction rates for
electrochemical reduction of CO₂ in organic electrolytes**

Journal:	<i>Green Chemistry</i>
Manuscript ID	GC-ART-01-2020-000013.R1
Article Type:	Paper
Date Submitted by the Author:	07-Feb-2020
Complete List of Authors:	Shaughnessy, Charles; The University of Kansas, Chemical & Petroleum Engineering Sconyers, David; University of Kansas, Department of Chemistry Lee, Hyun-Jin; University of Kansas, Department of Chemical and Petroleum Engineering Subramaniam, Bala; University of Kansas, Center for Environmentally Beneficial Catalysis Blakemore, James; University of Kansas, Department of Chemistry Leonard, Kevin; The University of Kansas, Chemical & Petroleum Engineering

Journal Name

ARTICLE TYPE

Cite this: DOI: 00.0000/xxxxxxxxxx

Insights into pressure tunable reaction rates for electrochemical reduction of CO₂ in organic electrolytes[†]Charles I. Shaughnessy,^{a,b} David J. Sconyers,^{a,c} Hyun-Jin Lee,^a Bala Subramaniam,^{*a,b} James D. Blakemore,^{*a,c} and Kevin C. Leonard^{*a,b}

Received Date

Accepted Date

DOI: 00.0000/xxxxxxxxxx

Electrochemical CO₂ reduction rates are limited in aqueous-based electrolytes by the low solubility of CO₂. We recently demonstrated that organic solvent-based CO₂ Expanded Electrolytes (CXEs) can solubilize multi-molar amounts of CO₂ at moderate pressures while retaining sufficient supporting electrolyte to facilitate electrochemistry. Up to an order of magnitude enhancement in CO₂ reduction rates to CO was achieved on polycrystalline Au electrodes at Faradaic efficiencies approaching 80%. Herein, we show that similar enhancements are observed on Cu catalysts as well, on the basis of enhanced current flow. On both systems, a maximum in CO₂ reduction rate was observed at ca. 5 M CO₂ concentration (i.e., 3.1 MPa head-space pressure) beyond which the rate decreases. To explain this counterintuitive phenomenon, we developed a detailed COMSOL-based mechanistic model of CO₂ reduction in organic electrolytes under elevated pressures on Au electrodes. This model incorporates the dissimilar variations of the key physicochemical properties (viz., CO₂ concentration, CO₂ diffusion rate, and solution polarity) with CO₂ pressure. We thereby demonstrate that the overall rate is limited by CO₂ concentrations at lower than optimum CO₂ pressures. At pressures higher than the optimum the rate is limited by both an attenuation of the first electron-transfer step and an increase in the ohmic resistance of the system. Excellent quantitative match between experimental and model-predicted rates lend credence to the proposed underlying mechanism of electrocatalytic CO₂ reduction in CXEs. These fundamental insights provide guidance for the rational design and scaleup of highly efficient CXE-based CO₂ reduction systems.

1 Introduction

Carbon dioxide (CO₂), a greenhouse gas that has been implicated in contributing to global climate change, also has potential as a valuable feedstock for making fuels and chemicals. However, the facile chemical activation of CO₂ remains a grand challenge in sustainability science.^{1–4} Of the many reported ways to convert CO₂, electrochemical CO₂ reduction is a promising method because it operates at low temperatures and can be powered by carbon-free renewable energy such as solar or wind.^{5–9} Even though several large-scale electrolysis technologies have been commercialized historically (e.g., the production of chlorine via the chlor-alkali process¹⁰ and the extraction of metals via electrowinning¹¹), the practical viability of electrochemical CO₂ re-

duction has thus far have been stymied by several technical obstacles.¹² One such roadblock is the poor solubility of CO₂ in conventional aqueous solvents.¹³ At ambient pressure, CO₂ solubility in aqueous electrolytes is approximately 0.034 M, and this low concentration limits the overall rate. Per Henry's Law, it is possible to linearly increase CO₂ concentration in aqueous media by simply increasing the head-space CO₂ pressure.¹⁴ However, even at the elevated pressures (e.g., 50 bars) investigated, the linear increase in CO₂ concentration is still too low in aqueous solvents to achieve practically relevant reaction rates.¹⁵ Thus, to increase CO₂ reduction rates, a system that uses other ways to enhance CO₂ availability at the electrode is needed.

Major improvements have been reported in CO₂ conversion rates by enhancing local CO₂ concentrations through the utilization of gas diffusion electrodes.^{16–20} Gas-diffusion electrodes allow for CO₂ reduction systems to be operated at current densities that are ca. ten times higher than those achieved using planar metal electrodes.¹⁹ Another attempted approach to enhance the CO₂ reduction rate is to engineer the catalyst surface with increased surface area and number of catalytically active sites.^{21–26} However, in all of these approaches, the low concentration of

^a Center for Environmentally Beneficial Catalysis, The University of Kansas, Lawrence, KS, USA

^c Department of Chemical & Petroleum Engineering, The University of Kansas, Lawrence, KS, USA

^c Department of Chemistry, The University of Kansas, Lawrence, KS, USA

*bsubramaniam@ku.edu; blakemore@ku.edu and kcleonard@ku.edu

[†] Electronic Supplementary Information (ESI) available: [details of any supplementary information available should be included here]. See DOI: 00.0000/00000000.

CO₂ in aqueous electrolytes may still be a critical impediment to achieving higher reaction rates.

To overcome the problem of CO₂ starvation at the electrode surface, we recently reported the use of CO₂-expanded solvents as reaction medium.²⁷ Upon CO₂ pressurization, the liquid phase volumetrically expands as the CO₂ concentration increases. The CO₂-expanded medium also sufficiently solubilizes supporting electrolyte in this range of pressures to facilitate electrochemistry.²⁷ Hence, we have termed these new electrochemical reaction media as CO₂-eXpanded Electrolytes (CXEs). Specifically, we have shown that at multi-molar CO₂ concentrations, tetrabutylammonium hexafluorophosphate remains in solution and fast outer-sphere electron-transfers (e.g., ferrocene/ferrocenium) can be carried out in CXEs across a wide range of CO₂ concentrations.²⁷ Most interestingly, we observed a non-monotonic pressure dependence of the CO₂ reduction rate (to CO) on polycrystalline Au in CXE media. We observed a maximum in CO₂ reduction rate at 3.1 MPa (corresponding to a CO₂ concentration of 5 M) representing an order of magnitude enhancement compared to the rate achieved at ambient pressure. At higher CO₂ pressures (and therefore higher liquid phase concentrations) exceeding this optimum, the electrochemical CO₂ activity decreases and eventually reaches values similar to that achieved at ambient pressure.

In this work, we have extended the CXE concept to CO₂ reduction with polycrystalline Cu catalysts to demonstrate the versatility of CXE media. On the Cu catalyst, we observed a similar non-monotonic change in CO₂ reduction rate with CO₂ head space pressure as seen on polycrystalline Au. Moreover, we observed that the optimum rate occurred at the same CO₂ concentration (ca. 5 M at 3.1 MPa head-space pressure) on both catalysts. Further, we present a complementary mathematical model that provides insights into the physicochemical processes underlying electrochemical CO₂ reduction in CXE media. The model successfully deconvolutes the pressure effects on the competing properties (liquid phase CO₂ concentrations, CO₂ diffusivity, and solution resistance) of CXEs that give rise to the experimentally observed maximum in electrocatalytic activity. These findings show that, in order to intensify electrochemical CO₂ reduction rates the reaction medium as well as the catalysts must be rationally designed to effectively harness the unique properties of CO₂-expanded electrolytes. These fundamental insights represents a significant advance in the effort to achieve practically relevant rates of CO₂ conversion for use in industrial-scale technologies.^{28,29}

2 Materials and Methods

Electrocatalytic CO₂ reduction experiments were performed in a custom fabricated pressure cell as previously described.²⁷ Briefly, a custom cap with threaded electrical feedthroughs was mated to a 50 mL Parr reactor to create the body of the cell. Commercially supplied liquid CO₂ (Matheson, Research Grade, purity level 99.9999%) was used to pressurize the vessel. Electrochemical data was collected using a Gamry Reference 3000 Potentiostat/Galvanostat. Cyclic voltammogram data for a gold microelectrode (0.000314 cm²) and a Cu (Alfa Aesar, 99.9%) disk electrode (0.0177 cm²) were obtained at various CO₂ head-

space pressures in acetonitrile containing dissolved tetrabutylammonium hexafluorophosphate (Sigma-Aldrich, electrochemical grade). The initial electrolyte concentration was 0.4 M. The volume of the liquid phase expands upon CO₂ dissolution at progressively higher pressures giving rise to a continuum of CXEs with tunable properties. The variations of the CXE volume and CO₂ concentrations in the CXEs were previously quantified in a Jurgeson[®] cell as described elsewhere.²⁷

3 COMSOL Simulation of CO₂ Electroreduction in CXEs

COMSOL (COMSOL Multiphysics[®] v. 5.3) simulations were used to model CO₂ electroreduction on a gold microelectrode in CXEs. The simulation field is shown in Supporting Information, Figure S1. The simulated reactor geometry was created as a 2D axial-symmetric domain with the electrode size (100 μm radius), insulating sheath size (10 μm width) and reactor dimensions (1 cm radius, 2 cm height). This reactor size was chosen because it is sufficiently larger than the boundary layer surrounding the electrode. Thus the CO₂ concentration at the outer boundary is the same as the reactor bulk concentration because of the limited diffusion profile around the microelectrode. A free triangular mesh using COMSOL's built-in 'normal' element size was used for the bulk of the reactor, with an 'extremely fine' mesh used for the area near the electrode (1.5mm x 2.5mm). An edge mesh was incorporated with a maximum mesh element of 2 × 10⁻⁵ cm and a minimum mesh element of 2 × 10⁻⁶ cm for increased spatial resolution near the electrode.

The concentration profiles of CO₂ and CO were simulated using the 'Transport of Diluted Species' module in COMSOL. This module uses Fick's law of diffusion [Equation (1)] to describe concentration gradients in the region around the electrode.

$$\frac{\partial C_i}{\partial t} = D_i \nabla^2 C_i \quad (1)$$

Experimentally measured initial CO₂ concentrations in CXEs at the various pressures were taken from our previous work.²⁷ The CO₂ diffusion coefficients in the CXE medium at various pressures were taken from values reported elsewhere.³⁰ 'No flux' boundary conditions were used at the reactor wall and insulation sheath of the electrode. A flux boundary condition for both CO₂ and CO was used at the electrode surface with the flux of each species governed by the reaction mechanism as shown in Table 1 (detailed description of the mechanism discussed in section 4.2). Specifically, the net flux of CO₂ is governed by the relative rates of the first and second reaction steps as shown in Equation (2).

$$J_{CO_2} = -r_1 - r_2 \quad (2)$$

Similarly the flux of CO is dependent on the reaction rate of the fourth step as shown in Equation (3).

$$J_{CO} = r_4 \quad (3)$$

The "Surface Reactions Physics" module in COMSOL was used to model the CO₂ reduction steps. The total site density was specified as 1.2 × 10⁻⁴ mol m⁻². Here the rate of formation of each

$\text{CO}_2 + \text{S}^* + \text{e}^- \xrightarrow{r_1} \text{CO}_2^{\bullet-}(\text{ads})$	$r_1 = k_1[\text{CO}_2][\text{S}^*]$	$k_1 = k_1^0 e^{-\alpha f(E-E^0)}$
$\text{CO}_2^{\bullet-}(\text{ads}) + \text{CO}_2 \xrightarrow{r_2} \text{OCOCO}_2^{\bullet-}(\text{ads})$	$r_2 = k_2[\text{CO}_2^{\bullet-}(\text{ads})][\text{CO}_2]$	
$\text{OCOCO}_2^{\bullet-}(\text{ads}) + \text{e}^- \xrightarrow{r_3} \text{CO}(\text{ads}) + \text{CO}_3^{2-}$	$r_3 = k_3[\text{OCOCO}_2^{\bullet-}(\text{ads})]$	$k_3 = k_3^0 e^{-\alpha f(E-E^0)}$
$\text{CO}(\text{ads}) \xrightarrow{r_4} \text{CO} + \text{S}^*$	$r_4 = k_4[\text{CO}(\text{ads})]$	

Where k^0 = Electron transfer kinetic rate constant, α = The transfer coefficient, $f = F/RT$
 E = Applied electrode potential, E^0 = Standard potential

Table 1. Elementary steps for the assumed electrochemical reduction of CO_2 on Au.

intermediate species (R_i) is described by Equations (4) to (6).

$$R_{\text{CO}_2^{\bullet-}(\text{ads})} = r_1 - r_2 \quad (4)$$

$$R_{\text{OCOCO}_2^{\bullet-}(\text{ads})} = r_2 - r_3 \quad (5)$$

$$R_{\text{CO}(\text{ads})} = r_3 - r_4 \quad (6)$$

Rate constant dependence on applied potential was taken into account by incorporating irreversible Butler-Volmer type kinetics into the kinetic rate constant as follows:

$$k_1 = k_1^0 e^{-\alpha f(E-E^0)} \quad (7)$$

where k_1^0 is the electron-transfer rate constant, $\alpha = 0.3$ is the transfer coefficient, E is the potential of the electrode, E^0 is an effective standard reduction potential, and $f = F/RT$ in which F is the Faraday constant, R is the gas constant, and T is temperature.

The current is calculated from the flux of electrons at the electrode surface as follows:

$$\frac{i}{nFA} = J_{e^-} = \frac{d[e^-]}{dt} = r_1 + r_3 \quad (8)$$

where A is the area of the electrode and n is number of electrons transferred in each reactions. Since this is a three dimensional model and the concentration profile is not necessarily constant across the electrode surface, thus the actual current is estimated as:

$$i = F \int_0^{2\pi} \int_0^a (r_1 + r_3) r' dr' d\theta \quad (9)$$

were a is the radius of the electrode.

The model uses the experimental potential versus time data from the cyclic voltammogram, and regresses the appropriate reaction rates and intermediate species concentrations at each time step. Once the current is calculated from Equation (9), the effect of the ohmic resistance is then determined. The experimental ohmic resistances at various pressures were measured using electrochemical impedance spectroscopy and used in the model for iR_u correction. The values of each k_i can then be found via regression by matching the simulated voltammogram to the experimental voltammogram.

4 Results and Discussion

4.1 Pressure Tunability of CXE Properties

As with CO_2 -eXpanded Liquids (CXEs),³¹ the physical properties of CXEs can be tuned by changing the CO_2 head-space pressure. Figure 1 shows the pressure-tunability of several key properties that affect electrocatalytic rates. Figure 1a shows that the volume of the electrolyte-containing acetonitrile solution expands exponentially as CO_2 dissolves into the liquid phase. At a pressure of ca. 5 MPa, the CXE volume expands up to three times its initial value. The corresponding liquid phase CO_2 concentrations in the CXE phase shown in Figure 1b. The CO_2 concentrations achievable in CXE media far exceed those attainable in aqueous electrolytes. For example, the CO_2 concentrations in water at 25 °C is 1.0 M at 3 MPa and 1.7 M at 5 MPa. In contrast, CO_2 concentrations in CXEs at 25 °C are 5 M and 13 M at 3 MPa and 5 MPa, respectively. In fact, CO_2 concentrations in CXEs approach that of pure liquid CO_2 (16.1 M) at 25 °C and pressures exceeding 5 MPa.

In addition to the pressure-tunability of CO_2 concentrations in CXEs, the CO_2 diffusion coefficient in CXEs also increases with CO_2 pressure. Figure 1c shows the variation of computed CO_2 diffusion coefficients in CO_2 -expanded acetonitrile with pressure.³⁰ Upon increasing CO_2 dissolution with pressure, the CXE transport properties trend towards becoming gas-like with a decrease in viscosity of the liquid phase and a concomitant increase in the CO_2 diffusion coefficient.

The increased CO_2 concentrations and improved CO_2 diffusion rates in CXEs would be expected to favor CO_2 electroreduction rates. However, the ohmic resistance of the Au/CXE system, as measured by electrochemical impedance spectroscopy with fitting to a Randles equivalent circuit (see Supporting Information Figures S2-S5), also increases with head-space CO_2 -pressure (Fig. 1d). This increase in resistance could inhibit the electron transfer rates associated with CO_2 electroreduction in CXEs. In sharp contrast, our previous experiments with a highly oriented pyrolytic graphite electrode show a negligible increase in resistance at increase CO_2 pressures.²⁷

We performed cyclic voltammetry over a wide range of CO_2 pressures for on both polycrystalline Au and Cu to better understand how the interplay between these pressure tunable properties affect the overall CO_2 electroreduction rates. We observed that for both catalysts, there was a non-monotonic relationship between CO_2 reduction activity and CO_2 pressure (Figure 2). On each electrocatalyst, we observed modest CO_2 reduction activ-

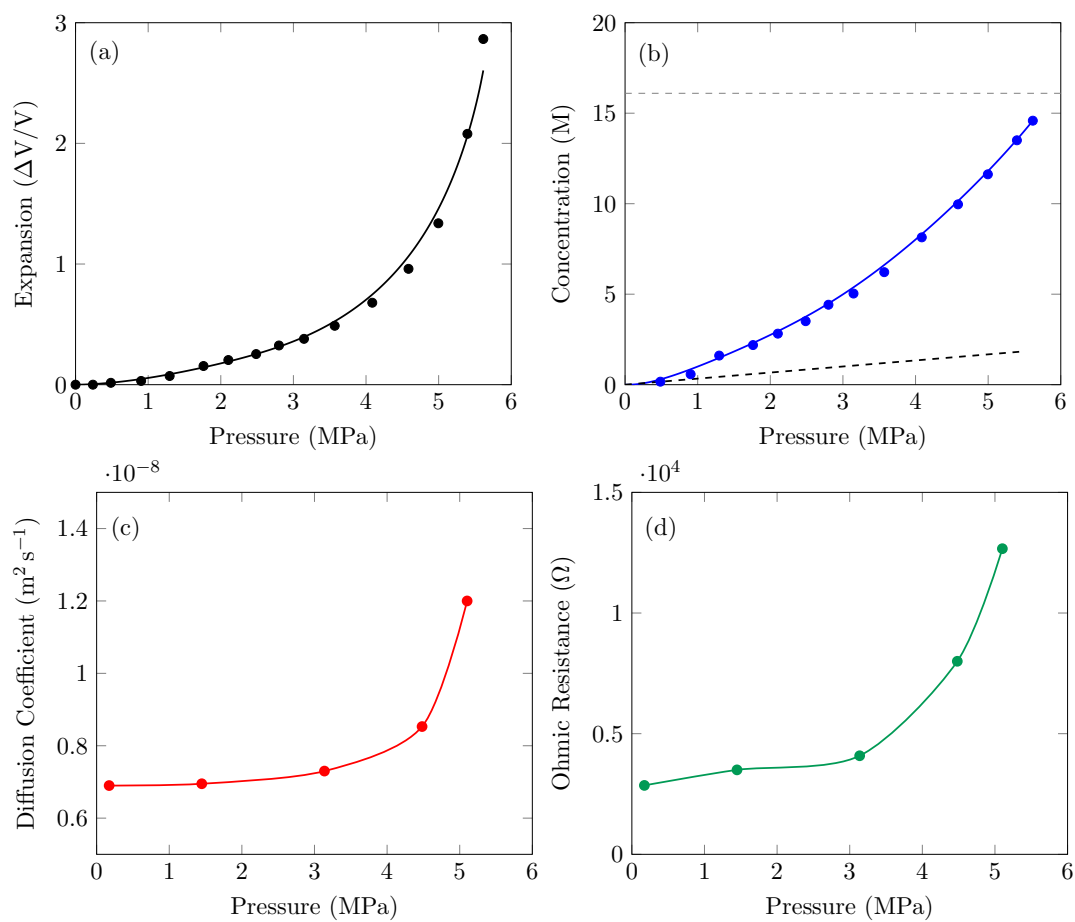


Fig. 1. Pressure dependant properties of CO₂-eXpanded Electrolytes. (a) Volumetric Expansion - experimental, (b) CO₂ concentration - experimental (blue - CXE, black - H₂O, gray - liquid CO₂), (c) Diffusion coefficient of CO₂ in CO₂-expanded acetonitrile - calculated³⁰, (d) CXE resistance with a Au microelectrode - experimental.

ity at near ambient CO₂ pressure (0.17 MPa). When the CO₂ pressure is increased to 3.13 MPa, there is a dramatic increase in the measured current. However, as the CO₂ pressure is increased beyond 3.1 MPa, there was an unexpected decrease in current density. At 5.1 MPa CO₂ pressure, the current density diminished approaching values observed at near ambient CO₂ pressures. This trend is preserved when the voltammograms are iR-corrected using the individual resistances measured at each pressure (Figure 2c). Interestingly, the shape of the voltammetry of the iR-corrected catalytic response at the optimum pressure is reminiscent of those observed during electrochemical hydrogen evolution in strong acid.³² This suggests that CO₂ availability is not limiting at these conditions.

In order to better understand the causative factors behind the occurrence of a maximum electrocatalytic CO₂ reduction rate at an intermediate CO₂ pressure, it is essential to deconvolute how the CO₂ concentration, CO₂ diffusion rate and ohmic resistance in the CXE medium are each affected by pressure. To accomplish this task, we employed the COMSOL simulation tool to model the CO₂ diffusion rate and CO₂ electroreduction kinetics. We chose to model the Au/CXE system because Au is well known to produce CO with high selectivity via a known mechanism.¹⁵ In contrast, Cu is known to make several gas and liquid-phase products, and

the CO₂ reduction mechanism on Cu catalysts is not as clear as on Au catalysts.¹⁵ However, we have confirmed that the formation of gas-phase product CO is attenuated at 5.1 MPa vs. 3.1 MPa in the Cu/CXE system (see Supporting Information Figures S7 and S8), in line with the corresponding electrochemical data. More systematic studies of the effects of operating conditions on product distribution for the Cu/CXE system are underway.

4.2 Mechanism of Electrochemical CO₂ Reduction in the CXE Media

To describe the CO₂ reduction kinetics, we went beyond the typical one-electron, Butler-Volmer approximation and developed a kinetic model that simulates each elementary reaction step in the electrocatalytic conversion of CO₂ to CO. The well-known mechanism, as described by Hori and co-workers, for CO₂ reduction on polycrystalline gold in aprotic, non-aqueous media is shown in Figure 3.¹⁵ The first step in this mechanism is the transfer of an electron to CO₂ to form an adsorbed CO₂^{•-} radical on the catalyst surface. A second CO₂ molecule then reacts with the adsorbed radical to form an adsorbed OCOCO₂^{•-} species. A subsequent electron transfer then forms free CO₃²⁻ and an adsorbed CO which then desorbs releasing the site to continue the

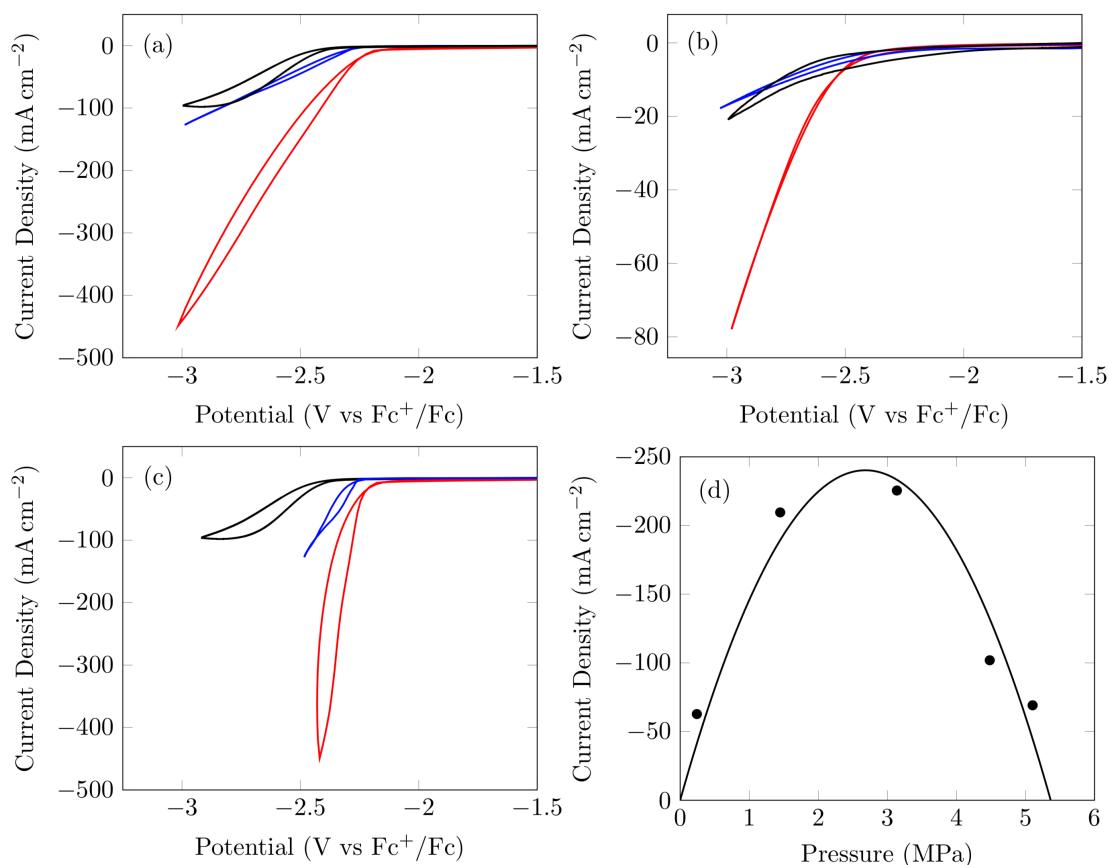


Fig. 2. Pressure dependant cyclic voltammograms (black - 0.2 MPa, red - 3.1 MPa, blue - 5.2 MPa). (a) CO₂ reduction on polycrystalline Au, (b) CO₂ reduction on polycrystalline Cu, (c) iR-corrected CO₂ reduction on polycrystalline Au, (d) Current density as a function of CO₂ pressure at -2.7 V vs Fc/Fc⁺ on polycrystalline Au.

catalytic cycle. It should be noted that while this catalytic cycle involves a two-electron transfer mechanism, it does not represent the two-electron, two-proton transfer mechanism that typically occurs in aqueous electrolytes. Furthermore, this model does not rely upon protons to be oxide acceptors as expected under our aprotic conditions. However, the product carbonate, a strong base under reaction conditions, is free to produce protons via Hoffman degradation with the supporting TBAPF₆ electrolyte in a non-rate determining step. Because we took precautions to maintain our reaction system to be devoid of protons via extensive drying of the electrolyte and utilization of high purity CO₂, the proposed mechanism should adequately capture the key features of CO₂ reduction in the CXE media.

Table 1 shows the equations used to describe the aforementioned electrochemical CO₂ reduction rates. The rate of the first reaction step, electron transfer to and adsorption of CO₂ on the catalyst surface, is taken to be first-order with respect to CO₂ concentration at the electrode surface and first-order with respect to the number of available sites, S* on the catalyst surface. The potential-dependent nature of this reaction step is taken into account by incorporating irreversible Butler-Volmer type kinetics [Equation (7)].

The rate of the second reaction step, CO₂ addition to the adsorbed CO₂^{•-} radical at the electrode surface to form OCOCO₂^{•-},

is also taken to be first-order in CO₂^{•-}_(ads) and first-order in CO₂ concentration at the electrode surface. The effective rate constant for this step that does not involve electron transfer is k_2 .

The rate of the third reaction step, the electron transfer to the adsorbed OCOCO₂^{•-}_(ads) radical to form CO with the release of carbonate, is taken to be first-order in OCOCO₂^{•-}_(ads). Analogous to the first step, k_3 is dependent on the electrode potential as per irreversible Butler-Volmer kinetics. The final step in the mechanism is the desorption of CO which is assumed to be first order with respect to CO_(ads).

Employing this kinetic model, we simulated the cyclic voltammetry data at various pressures by regressing the kinetic parameters for each reaction step. As discussed earlier, values of CO₂ diffusion coefficients, CO₂ concentrations, scan rate, and CXE ohmic resistance are either measured or estimated at each pressure and are supplied as model inputs. The k_i values for each reaction were regressed to fit the experimental data. As shown in Figure 4, excellent fits of the simulated and experimental cyclic voltammetry data for polycrystalline Au were obtained at CO₂ pressures of 0.17, 1.44, 3.13, 4.48, and 5.10 MPa. The known and regressed parameters are shown in Table 2.

The regressed parameters provide insights into why an optimum exists for electrochemical CO₂ reduction as a function of CO₂ head-space pressure. The increased resistance of the system

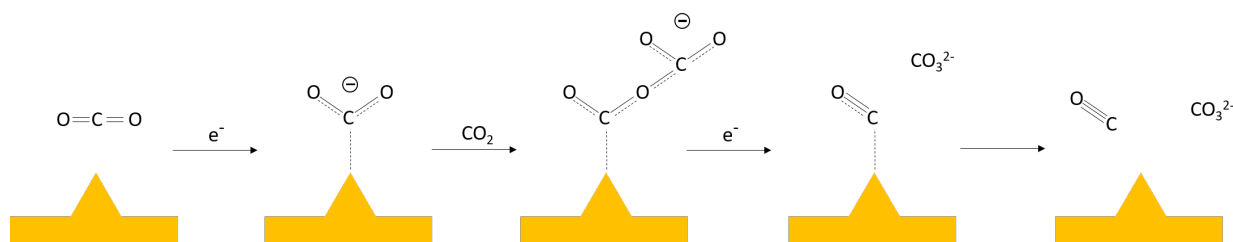


Fig. 3. Illustrative reaction mechanism for the electrochemical reduction of CO₂ on Au.

Pressure	(*Input Parameters †Regressed Parameters)							
	C_0 [M]*	D [m ² s ⁻¹]*	R_{sys} [Ω]*	k_1^0 [m ³ mol ⁻¹ s ⁻¹] [†]	k_2 [m ³ mol ⁻¹ s ⁻¹] [†]	k_3 [s ⁻¹] [†]	k_4 [s ⁻¹] [†]	
0.17 MPa	0.08	6.9×10^{-9}	2856	2×10^{-8}	100	8×10^{-5}	500	
1.44 MPa	1.47	6.95×10^{-9}	3500	2×10^{-8}	100	8×10^{-5}	500	
3.13 MPa	5	7.3×10^{-9}	4085	2×10^{-8}	100	8×10^{-5}	500	
4.48 MPa	9.64	8.52×10^{-9}	8000	0.2×10^{-8}	100	8×10^{-5}	500	
5.10 MPa	13	12×10^{-9}	12666	0.1×10^{-8}	100	8×10^{-5}	500	

Table 2. Input and regressed parameters for the COMSOL model.

at higher CO₂ pressures partially explains the observed maximum in the electrochemical CO₂ reduction rates. While the increased resistance causes a decrease in the slope of the catalytic wave, it is not responsible for the change in the onset potential to more negative potentials. That change in onset potential is due to the decrease in the rate constant associated with the first step (k_1^0) with increasing CO₂ pressure. These results are consistent with the equivalent circuit modelling of the EIS data, which shows essentially no change in the charge-transfer resistance between atmospheric conditions and 3.1 MPa, but an order of magnitude increase in the charge-transfer resistance between 3.1 MPa and 5.1 MPa (See Supporting Information for details, and Tables S1-S3 for the resistance values.). We observed no change in the values of the apparent rate constants for the second, third, and fourth elementary reaction over the pressure range.

The model results also provide several key insights into the rate-determining steps of electrochemical CO₂ reduction, that are not discernible by experiments carried out solely at ambient CO₂ concentration. First, the model demonstrates that under ambient pressure, r_1 (the first electron-transfer step) is the rate-determining step at all potentials. To elucidate rate-determining steps, we assumed different kinetic rate constants for each of the four mechanistic steps. The response of a catalyst at ambient CO₂ pressure, starting with the k_i values found for Au, and varying each k_i value one at a time across several orders of magnitude was investigated (see Supporting Information, Figure S9). Increasing the value of k_1^0 while maintaining k_2 , k_3^0 , and k_4 values constant improves the catalyst performance at low (i.e., less negative) potentials for CO production (see Figure S9a). In contrast, increasing k_2 , k_3^0 , or k_4 , while maintaining k_1^0 constant, does not increase the rate of CO formation, indicative of r_1 being rate-determining (see Figures S9b-S9d). However, the reason for r_1 limiting the overall rate is different at lower (i.e. less negative) potentials than at higher (i.e. more negative) potentials. At low potentials, the kinetics of the electron transfer (i.e., k_1) are lim-

iting the rate of reaction as demonstrated by the theoretical shift in the onset potential for electrochemical CO₂ reduction to less negative potentials. However, at high potentials (i.e., more negative), the maximum attainable current is the same regardless of the value of k_1^0 . Recall that r_1 is expressed as:

$$r_1 = k_1[\text{CO}_2][\text{S}^*] \quad (10)$$

where k_1 is a function of potential as described in eq. (7). Thus, at high potentials, the overall rate is limited not by the value of k_1 but rather by either the CO₂ concentration at the electrode surface and/or $[\text{S}^*]$, the concentration of unoccupied surface sites.

Figure 5a shows simulations of theoretical catalysts under ambient CO₂ pressure keeping all values of the k_i found for Au, but increasing the total number of available catalytic sites. Again, under more negative potentials, the rate of reaction (i.e., current) is the same regardless of the catalytic site density. This unequivocally shows that CO₂ concentration at the electrode surface limits the overall CO₂ reduction at ambient conditions.

At the optimum CO₂ pressure (3.1 MPa), the overall rate is dictated by the electron-transfer kinetics (both k_1^0 and k_3^0) as well as the overall catalyst site density. Unlike at ambient CO₂ pressure, increasing only k_1^0 does not increase the overall rate of reaction. In fact, when the k_i values are varied one at a time it is not possible to significantly increase the rate of reaction simply by increasing only one rate constant (see Supporting Information, Figure S10). However, keeping all of the k_i values identical to those found for Au, but increasing the catalytic site density (Figure 5b) does show a significant increase in the theoretical performance. This demonstrates that, contrary to under ambient pressure conditions, CO₂ concentration at the electrode surface does not limit the overall rate when the bulk CO₂ concentration is at ca. 5 M. Under these conditions, the reaction rate is mainly limited by the number of catalytic sites available.

Additional gains in catalytic activity can be made at the optimum CO₂ pressure if a catalyst could be designed to increase

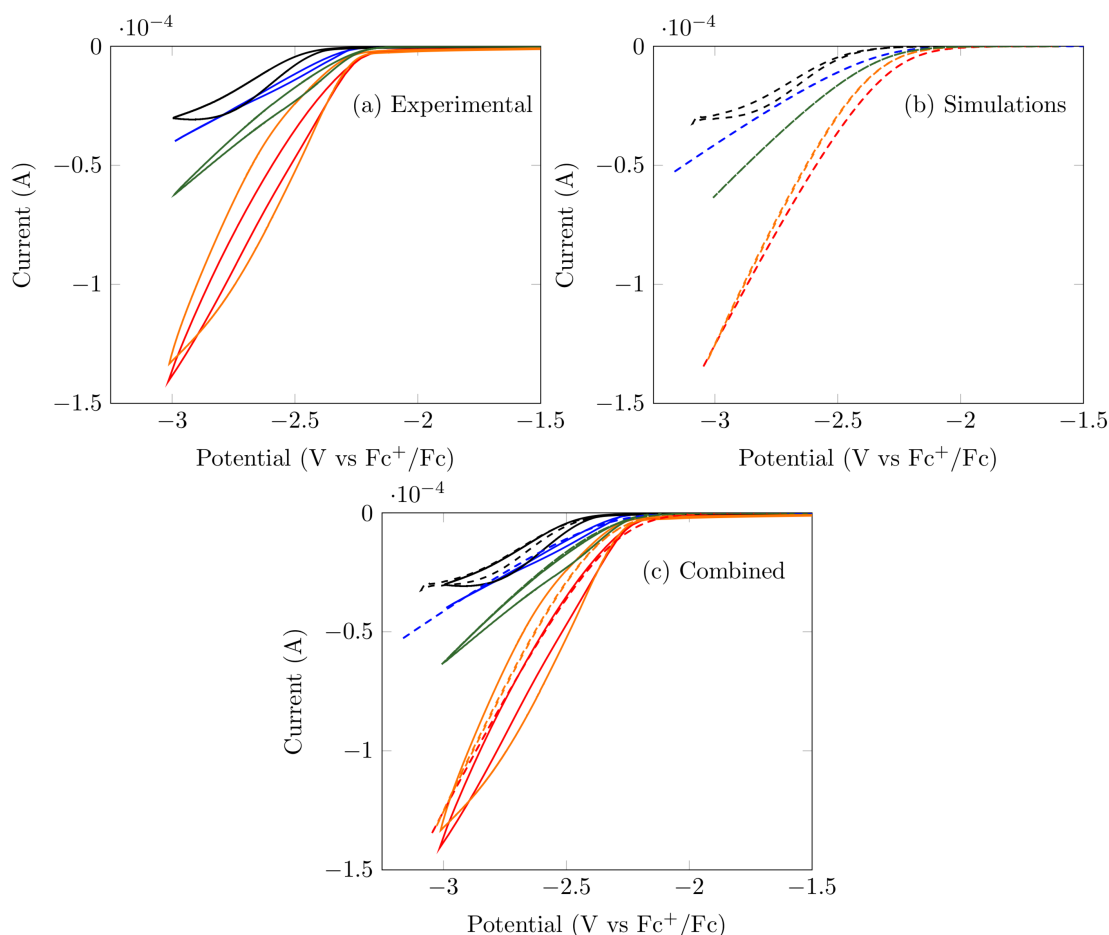


Fig. 4. Pressure dependant cyclic voltammograms for the electrochemical reduction of CO_2 on Au. (a) Experimental, (b) Simulated, (c) Combined. (Black 0.17 MPa, Orange 1.44 MPa, Red 3.13 MPa, Green 4.48 MPa, Blue 5.10 MPa)

both k_1^0 and k_3^0 simultaneously (see Supporting Information, Figure S12b). At 3.1 MPa, an initial increase in k_1^0 does not show a dramatic effect on the electrochemical CO_2 reduction activity; however, an increase in k_3^0 enhances catalyst performance. In sharp contrast, at ambient pressure (Supporting Information, Figure S12a), increasing k_1^0 will increase catalytic activity, but a subsequent increase in k_3^0 does not offer additional performance enhancements. This signifies that in order to increase CO_2 reduction rates under the optimum CO_2 concentration, a catalyst needs to be designed with increased number of catalytic sites that favor fast electron-transfer kinetics for both the first and third steps. Under ambient pressure conditions, a catalyst need only be designed to have fast electron-transfer kinetics for the first step. The number of sites nor the kinetics of the subsequent steps do not have significant effects at ambient pressure. Thus, combining higher active site density catalysts with a CXE is a better strategy for higher CO_2 reduction rates than under ambient pressure conditions.

At the highest CO_2 pressures tested, the overall rate is controlled by the sluggish electron-transfer kinetics of the first step and the resistivity of the system (see Supporting Information, Figure S11). This can be seen by the increased catalytic activity at increased values of k_1^0 . However, there is a point beyond which in-

creasing the value of k_1^0 alone does not keep improving the overall performance of the system, analogous to the intermediate pressure regime.

5 Conclusion

This study has elucidated the various competing effects on electrochemical CO_2 conversion rates as the liquid-phase CO_2 concentration is increased in CO_2 -rich acetonitrile-based electrolytes. We observed a maximum in the electrochemical CO_2 reduction rate at an intermediate optimum CO_2 concentration (i.e., pressure). Beyond the optimum, the higher CO_2 concentrations increase the ohmic resistance of the system and also inhibit the kinetics of the first electron-transfer step. Fortunately, the optimum pressure (3.13 MPa) at which the electrocatalytic reduction rate is maximized is quite mild and in the range of many current industrial chemical processes. The existence of an optimum CO_2 concentration has important implications for rationally designing electrochemical CO_2 reduction systems. The simulations clearly show that sophisticated nanostructured catalysts may not be able to fully utilize their high active site density at CO_2 concentrations below the optimum. Further, the systematic design of compatible electrolyte/solvent/catalyst combination will be essential for achieving practically relevant electrochemical CO_2 reduction

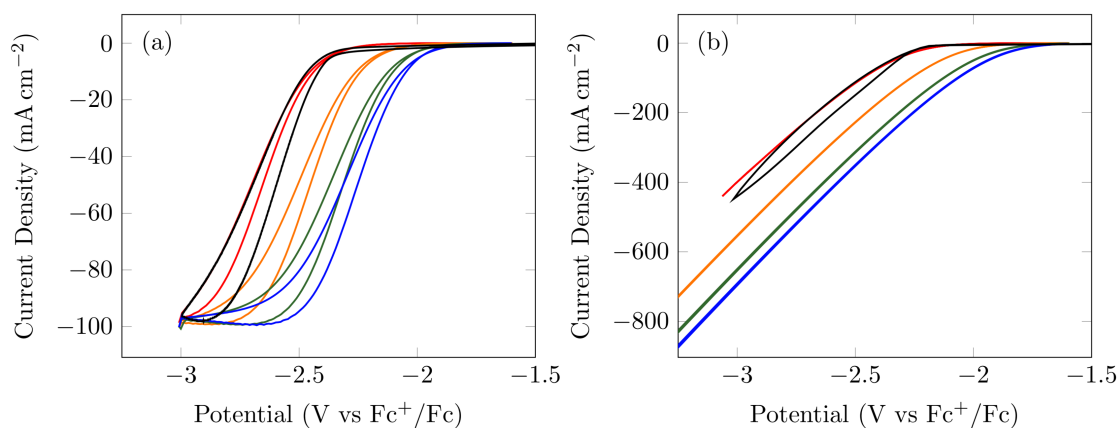


Fig. 5. Simulated cyclic voltammograms of theoretical catalysts at various catalytic site densities (red - $1.2 \times 10^{-4} \text{ molm}^{-2}$, orange - $12 \times 10^{-4} \text{ molm}^{-2}$, green - $60 \times 10^{-4} \text{ molm}^{-2}$, blue - $120 \times 10^{-4} \text{ molm}^{-2}$, black - Experimental on polycrystalline Au) at both ambient pressure (a) and 3.1 MPa (b)

rates.

Conflicts of interest

There are no conflicts to declare.

Acknowledgements

This work was supported by the US National Science Foundation through award CBET-1605524.

References

- 1 A. M. Appel, J. E. Bercaw, A. B. Bocarsly, H. Dobbek, D. L. DuBois, M. Dupuis, J. G. Ferry, E. Fujita, R. Hille, P. J. A. Kenis, C. A. Kerfeld, R. H. Morris, C. H. F. Peden, A. R. Portis, S. W. Ragsdale, T. B. Rauchfuss, J. N. H. Reek, L. C. Seefeldt, R. K. Thauer and G. L. Waldrop, *Chem. Rev.*, 2013, **113**, 6621–6658.
- 2 J. H. Montoya, L. C. Seitz, P. Chakthranont, A. Vojvodic, T. F. Jaramillo and J. K. Nørskov, *Nat. Mater.*, 2017, **16**, 70.
- 3 G. Fiorani, W. Guo and A. W. Kleij, *Green Chem.*, 2015, **17**, 1375–1389.
- 4 D. L. DuBois, *Inorg. Chem.*, 2014, **53**, 3935–3960.
- 5 D. T. Whipple and P. J. A. Kenis, *J. Phys. Chem. Lett.*, 2010, **1**, 3451–3458.
- 6 D. D. Zhu, J. L. Liu and S. Z. Qiao, *Adv. Mater.*, 2016, **28**, 3423–3452.
- 7 C. Costentin, M. Robert and J.-M. Savéant, *Chem. Soc. Rev.*, 2013, **42**, 2423–2436.
- 8 Z.-Q. Liang, T.-T. Zhuang, A. Seifitokaldani, J. Li, C.-W. Huang, C.-S. Tan, Y. Li, P. De Luna, C. T. Dinh, Y. Hu, Q. Xiao, P.-L. Hsieh, Y. Wang, F. Li, R. Quintero-Bermudez, Y. Zhou, P. Chen, Y. Pang, S.-C. Lo, L.-J. Chen, H. Tan, X. Zheng, S. Zhao, D. Sinton and E. H. Sargent, *Nat. Commun.*, 2018, **9**, year.
- 9 J. Wang, S. Kattel, C. J. Hawxhurst, J. H. Lee, B. M. Tackett, K. Chang, N. Rui, C.-J. Liu and J. G. Chen, *Angew. Chem., Int. Ed.*, 2019, **58**, 6271–6275.
- 10 R. K. Karlsson and A. Cornell, *Chem. Rev.*, 2016, **116**, 2982–3028.
- 11 A. Alfantazi and R. Moskalyk, *Miner. Eng.*, 2003, **16**, 687–694.
- 12 J. Qiao, Y. Liu, F. Hong and J. Zhang, *Chem. Soc. Rev.*, 2014, **43**, 631–675.
- 13 Y. Chen, N. S. Lewis and C. Xiang, *Energy Environ. Sci.*, 2015, **8**, 3663–3674.
- 14 Z. Duan and R. Sun, *Chem. Geol.*, 2003, **193**, 257–271.
- 15 Y. i. Hori, *Mod. Aspects Electrochem.*, Springer, 2008, pp. 89–189.
- 16 D. T. Whipple, E. C. Finke and P. J. Kenis, *Electrochem. Solid-State Lett.*, 2010, **13**, B109–B111.
- 17 S. Verma, Y. Hamasaki, C. Kim, W. Huang, S. Lu, H.-R. M. Jhong, A. A. Gewirth, T. Fujigaya, N. Nakashima and P. J. Kenis, *ACS Energy Lett.*, 2017, **3**, 193–198.
- 18 R. L. Cook, R. C. MacDuff and A. F. Sammells, *J. Electrochem. Soc.*, 1990, **137**, 607–608.
- 19 N. Furuya, T. Yamazaki and M. Shibata, *J. Electroanal. Chem.*, 1997, **431**, 39–41.
- 20 B. Endrődi, G. Bencsik, F. Darvas, R. Jones, K. Rajeshwar and C. Janáky, *Prog. Energy Combust. Sci.*, 2017, **62**, 133–154.
- 21 Y. Chen, C. W. Li and M. W. Kanan, *J. Am. Chem. Soc.*, 2012, **134**, 19969–19972.
- 22 H.-E. Lee, K. D. Yang, S. M. Yoon, H.-Y. Ahn, Y. Y. Lee, H. Chang, D. H. Jeong, Y.-S. Lee, M. Y. Kim and K. T. Nam, *ACS Nano*, 2015, **9**, 8384–8393.
- 23 H. Mistry, R. Reske, Z. Zeng, Z.-J. Zhao, J. Greeley, P. Strasser and B. R. Cuenya, *J. Am. Chem. Soc.*, 2014, **136**, 16473–16476.
- 24 S. Mostafa, F. Behafarid, J. R. Croy, L. K. Ono, L. Li, J. C. Yang, A. I. Frenkel and B. R. Cuenya, *J. Am. Chem. Soc.*, 2010, **132**, 15714–15719.
- 25 W. Zhu, Y.-J. Zhang, H. Zhang, H. Lv, Q. Li, R. Michalsky, A. A. Peterson and S. Sun, *J. Am. Chem. Soc.*, 2014, **136**, 16132–16135.
- 26 X. Feng, K. Jiang, S. Fan and M. W. Kanan, *J. Am. Chem. Soc.*, 2015, **137**, 4606–4609.
- 27 C. Shaughnessy, D. Sconyers, T. Kerr, H.-J. Lee, B. Subrama-

- niam, K. Leonard and J. Blakemore, *ChemSusChem*, 2019, **12**, 3761–3768.
- 28 J. H. Montoya, C. Shi, K. Chan and J. K. Nørskov, *J. Phys. Chem. Lett.*, 2015, **6**, 2032–2037.
- 29 J. Rosen, G. S. Hutchings, Q. Lu, S. Rivera, Y. Zhou, D. G. Vlachos and F. Jiao, *ACS Catal.*, 2015, **5**, 4293–4299.
- 30 Y. Houndonougbo, B. B. Laird and K. Kuczera, *J. Chem. Phys.*, 2007, **126**, 074507.
- 31 P. G. Jessop and B. Subramaniam, *Chem. Rev.*, 2007, **107**, 2666–2694.
- 32 W. Sheng, Z. Zhuang, M. Gao, J. Zheng, J. G. Chen and Y. Yan, *Nat. Commun.*, 2015, **6**, 5848.